The Software Package AIRY 7.0: new efficient deconvolution methods for post-adaptive optics data

Andrea La Camera[a], Marcel Carbillet[b], Marco Prato[c], Patrizia Boccacci[a], and Mario Bertero[a]

[a]Dipartimento di Informatica, Bioingegneria, Robotica e Ingegneria dei Sistemi (DIBRIS), Università di Genova, Via Dodecaneso 35, 16145 Genova, Italy
[b] Laboratoire Lagrange, Université de Nice Sophia-Antipolis/Observatoire de la Côte d'Azur/CNRS, Parc Valrose, 06100 Nice, France
[c]Dipartimento di Scienze Fisiche, Informatiche e Matematiche, Università di Modena e Reggio Emilia, Via Campi 213/b, 41125 Modena, Italy

ABSTRACT

The `Software Package AIRY` (acronym of Astronomical Image Restoration in interferometrY) is a complete tool for the simulation and the deconvolution of astronomical images. The data can be a post-adaptive-optics image of a single dish telescope or a set of multiple images of a Fizeau interferometer. Written in IDL and freely downloadable, `AIRY` is a package of the `CAOS Problem-Solving Environment`. It is made of different modules, each one performing a specific task, e.g. simulation, deconvolution, and analysis of the data. In this paper we present the last version of `AIRY` containing a new optimized method for the deconvolution problem based on the scaled-gradient projection (SGP) algorithm extended with different regularization functions. Moreover a new module based on our multi-component method is added to `AIRY`. Finally we provide a few example projects describing our multi-step method recently developed for deblurring of high dynamic range images. By using `AIRY` v.7.0, users have a powerful tool for simulating the observations and for reconstructing their real data.

Keywords: Software Package AIRY, CAOS Problem-Solving Environment, Image deconvolution, Scaled Gradient Projection algorithm, Multi-component method, Multi-step method

1. INTRODUCTION

The idea of developing a software tool for the simulation and the reconstruction of the images of the future Fizeau interferometers of the Large Binocular Telescope (LBT) was the result of a discussion of a group of astronomers, physicists and mathematicians during a coffee break of the 2000 SPIE conference in Munich.

The focus on interferometry is indicated in the acronym of the software, AIRY from Astronomical Image Restoration in interferometrY. The first version was described in a paper published two years later[1]. The deconvolution methods contained in this first version were based on the extension of the Richardson-Lucy (RL)[2,3] method and of the Iterative Space Reconstruction Algorithm (ISRA)[4].

Since then, the software was expanded in several directions mainly as concerns the image reconstruction methods. In the framework of the RL approach, regularization methods with different kinds of regularization and blind deconvolution methods were proposed, tested and inserted in the tool. Moreover, the case of spectra deconvolution was also included. Already in its present form, version 7.0 `AIRY` can be considered the most complete public software for image simulation and restoration, since the methods for multiple image deconvolution (Fizeau interferometry) can also be applied to the case of a single image.

The `Software Package AIRY` is a package of the `CAOS Problem-Solving Environment`[5,6] (in short, `CAOS PSE`), and it is written in IDL. The `CAOS PSE` has been recently renewed and details about its new version (7.0 as well) are given in next section. A paper presenting the new version of the companion package of adaptive

Further author information: (Send correspondence to A.L.C., M.C.)
A.L.C.: E-mail: andrea.lacamera@unige.it, Telephone: +39 010 353 6609
M.C.: E-mail: marcel.carbillet@unice.fr, Telephone: +33 (0)4 92 07 63 28

optics systems modeling, the Software Package CAOS, benefitting also from the renewal of the whole CAOS PSE, is presented at this conference[7].

The paper is organized as follows. In sect.2 we describe the main modifications of the software due to the mentioned new version of the CAOS PSE; then we briefly describe the modules of the package and next we give a summary of the deconvolution methods present in AIRY. In sect.3 we show the multi-component deconvolution module, a new module introduced in this version of AIRY and consisting in a method already published by our group[8]. For the convenience of the reader we outline the algorithm at the beginning of the section. In sect.4 we introduce the multi-step method, specifically developed for deconvolving Io images taken by Keck-II and Large Binocular Telescope (LBT) in recent years. In sect.5 we sketch the conclusions and we give ideas of future developments of the software.

2. THE NEW VERSION OF AIRY

2.1 Adapting AIRY to the new CAOS PSE

Together with this new version of the Software Package AIRY, a complete renewal of the whole CAOS PSE has been performed. The common components of the CAOS PSE — the CAOS Application Builder[9], consisting in the code of its global user interface, the CAOS Library, a series of utility routines, and the CAOS Template Module, a template for developing new modules within the packages — are now unified into a simplified software structure with one only version distribution of the CAOS PSE. The installation procedure has been so simplified as well, and utility modules developed in different packages have been regrouped within it. The working directory, where users can develop their own simulation and data processing projects through the global user interface, was also regrouped into this new simplified structure. The new CAOS PSE ends so up within a unique main directory with its global user interface, its utility routines library, its working directory (or directories if using different packages) with dedicated example projects detailing the practical use of each module, and finally the installed scientific packages (the Software Package CAOS, the Software Package AIRY) together with some utility modules for displaying/reading/writing input/output data and a template module. Some debuggings, enhancements, and global simplifications have been also performed *en passant*.

As a consequence of these global changings, the utility modules of the past distributions of the Software Package AIRY (mainly DSP for displaying data, WFT for writing images, and RFT for reading images) were moved to the new common utility modules of the CAOS PSE, merged with utility modules from other packages, and are now distributed within it. Note that scientific packages such as the Software Package CAOS and the Software Package AIRY are still distributed in a separate manner.

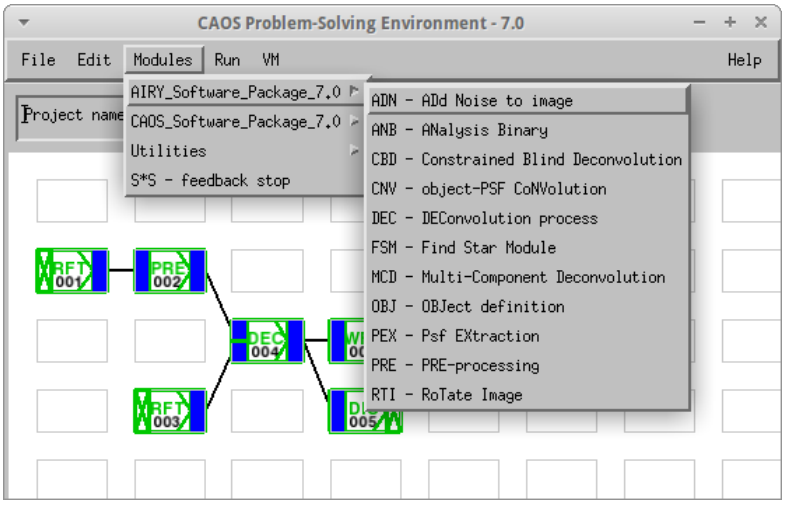

Figure 1. Example of use of the global user interface of the CAOS PSE together with some basic modules of the Software Package AIRY and utility modules. The list of modules of the Software Package AIRY, appearing when clicking on button Modules, is also shown.

In Fig. 1 we show an example of the use of the global user interface of the CAOS PSE together with some basic modules of the Software Package AIRY and utility modules. The project shown in the worksheet is a simple deconvolution implying image and PSF data read through module RFT, pre-processed through module PRE, deconvolved through module DEC, and then displayed and saved thanks to the utility modules DIS and WFT.

2.2 Description of the Software Package

The new version of the Software Package AIRY is made of 11 modules, each one being specifically designed to perform a task. The modules are placed on the worksheet of the CAOS PSE and the output of a module can be linked to (one or more links of) another module. Two different data types are defined in AIRY: one for sources (used in the object definition and convolution modules) that is called src_t and the other one for the images, called img_t. After the rebuilding of the whole CAOS PSE, several modules have been moved to the Utilities and therefore we can order the remaining modules in three subsets: simulation modules, deconvolution modules, and data analysis modules. In Tab. 1 we show each module and its use within AIRY.

Table 1. The 11 modules of AIRY version 7.0, divided in three subsets, depending on the goal of each module (shown in the last column).

Module	Purpose	Goal
OBJ	OBJect definition	Simulation
CNV	CoNVolution between object and psf	
ADN	ADd Noise to image	
PRE	PREprocessing data	Deconvolution
DEC	DEConvolution	
MCD	Multi-Component Deconvolution [NEW!]	
CBD	Constrained Blind Deconvolution	
PEX	Psf extraction and EXtrapolation	
RTI	RoTate Image	
ANB	ANalysis Binary stars	Data Analysis
FSM	Find Stars Module	

It is evident from the table that the main goal of AIRY is deconvolution. Indeed, in the previous version of AIRY we improved the CBD module containing two methods for Strehl Constrained blind deconvolution[10–13]. In this version several improvements of the module DEC (as described in the next section) are made. Moreover a new module (MCD) contains a recently developed method for deconvolving high-dynamic range images (e.g. jets from young stars[8,14]).

Another important modification performed within the whole package concerns the sky background evaluation. Thanks to the updates to the PRE module, the sky background can now be stored in an array that can be either loaded from a FITS file or defined by a constant value (automatically computed or inserted by the user in the text field of the GUI). This information is saved in the img_t structure and used by other modules.

A new feature of AIRY is the intense use of the FITS header. As it is known, a lot of information is usually contained here and this is now preserved from the beginning to the end of the pipeline. Moreover, information about simulation and/or deconvolution (and other tasks performed by the software) are saved in the header. Every new keyword added by a module has a comment with the name of the module itself in square brackets, in order to be easily recognized by the user. There are specific keywords for the two data structures of AIRY. In Tab. 2 we describe the most important keywords used by the software and the corresponding module adding the keyword. We also include the keywords used in AIRY modules, but added from other modules (e.g. of the package Utilities, as described in the previous section). Together with the package a complete and updated list of the keywords is distributed.

2.3 Deconvolution methods contained in DEC

In previous papers[15–17] we already described the general approach to the deconvolution problem. Within AIRY three methods for reconstructing images in the case of Poisson data are implemented: the mentioned RL, its version for multiple images, the Ordered-Subset Expectation Maximization (OSEM) algorithm[18], and the

Table 2. The most important/used keywords in AIRY. The last column shows the module that introduces the keyword. The complete list of keywords is available within AIRY.

Keyword	Description	Module
OBJECT	Object simulated	OBJ
BAND	Filter band	OBJ
PIX_SIZE	Pixel size [arcsec]	OBJ
APTAREA	Aperture area [m^2]	CNV
EFF_ALL	Overall efficiency	CNV
EXPTIMEn	Exposure time [s] for image n	CNV, WFT
SKY_TYPE	Sky background type (File or Values)	ADN, PRE, PEX
SKY_FILE	Sky background filename	ADN, PRE, PEX
SKY_NB	Number of background values	ADN, PRE, PEX
SKY_BGn	Sky background value for image n	ADN, PRE, PEX
POISSON	Poisson noise on the image	ADN
RON	Read out noise value [e^-/px]	ADN, PRE
GAIN	Gain of the CCD [e^-/ADU]	ADN, PRE
PSF_EXTR	PSF extracted / estrapolated	PEX
MOFFAT	Moffat exponent of the PSF	PEX
METHOD	Deconvolution method	DEC, MCD
BOUND	Boundary effects correction	DEC, MCD
EE_TRESH	Enclosed Energy threshold	DEC, MCD
FLUX_CON	Flux constraint - used by SGP	DEC, MCD
REG_TYPE	Regularization function	DEC, MCD
REG_BETA	Regularization parameter (β)	DEC, MCD
REG_DELT	Regularization parameter (δ)	DEC, MCD
STOP_CRI	Stopping rule number	DEC, MCD
STOP_TOL	Stopping tolerance	DEC, MCD
ITER	Number of iterations	DEC, MCD
CBD_ALG	Blind Deconvolution algorithm	CBD
STREHL_C	Apply the Strehl Constraint	CBD
SRn	Strehl value of the image n	CBD
PSF_INIT	PSF initialization	CBD
ROT_TYPE	Rotation method	RTI
NB_ANGLES	Number of angles	RTI
ANGLEn	Angle of the image n	RTI
NPIXEL	Size of the working array	WFT
RESOLUT	Plate scale [arcsec/px]	WFT
LAMBDA	Central wavelenght of the filter [Å]	WFT
WIDTH	Width of the filter [Å]	WFT

recently added Scaled Gradient Projection (SGP) method[19]. Moreover we also have the ISRA algorithm used in the case of Gaussian data, and its extension to multiple images called OS-ISRA.

Each one of the mentioned methods has several extensions, depending on the current problem. In the case of RL/OSEM algorithms, since they are relatively slow, the user can use an accelerated version based on Biggs and Andrews approach[20,21]. In addition, it is possible to increase the super-resolution effect of the RL and OSEM algorithms by using a suitable initialization of the method[22,23]. In all methods, when the object has an angular size greater than the field of view of the instrument, the boundary effect correction[24,25] can be applied. Moreover, a set of regularizations[26] are integrated in the previous version of AIRY for all the methods except SGP, while in Prato et al[27] SGP has been extended with several regularizations.

In this work we focus on Poisson data and in particular on the SGP method. We tested this method in several papers[19,28–31], not only within AIRY, and in this version of the package SGP is selected as the default method for deconvolution. For the convenience of the reader we recall here the model of image formation and we sketch the deconvolution problem.

We denote by $\mathbf{f} = \mathbf{f}(\mathbf{n})$ the unknown science object to be reconstructed and by $\mathbf{g} = \mathbf{g}(\mathbf{m})$ the image. In the case of multiple image, if p is the number of observations, then $\mathbf{g} = \mathbf{g}_1, \ldots, \mathbf{g}_p$. Moreover, in order to take into account the boundary effect corrections, we denote by $\mathbf{n} = \{n_1, n_2\} \in R$ the multi-index varying on the pixels of the object domain R and by $\mathbf{m} \in S$ the multi-index of the pixels in the image domain S. We suppose that R is broader than S and we extend both to a broader array $\bar{S}$ by zero-padding. The model of image formation (see eq (1) in[17]) is the sum of three components, the first two are given by the number of photons arising from the object and the background and are described by a Poisson process, while the last one is the Read-Out Noise (RON), described by a Gaussian process with zero mean and variance σ^2. According to Snyder et al.[32] the RON is approximated by a Poisson process so that we can assume only Poisson data by adding the variance σ^2 of the RON to the detected image and to the background. The model is therefore:

$$\mathbf{g}_j(\mathbf{m}) = (A_j\mathbf{f})(\mathbf{m}) + \mathbf{b}_j(\mathbf{m}) \quad , \quad j = 1, \ldots, p \tag{1}$$

where A_j is the imaging matrix defined by $A_j\mathbf{f} = \mathbf{K}_j * \mathbf{f}$ (in the case of space-invariant images) and $\mathbf{b}_j$ is the sky background array. Here $\mathbf{K}_j$ is the j-th point-spread function (PSF) of the system and $*$ denotes the convolution product. The general Bayesian approach to the deconvolution problem leads to the minimization of the regularized functional

$$J_\beta(\mathbf{f}; \mathbf{g}) = J_0(\mathbf{f}; \mathbf{g}) + \beta J_1(\mathbf{f}) \quad , \tag{2}$$

where the data-fidelity function $J_0(\mathbf{f}; \mathbf{g})$ is the so-called Kullback-Leibler divergence (or Csiszár I-divergence[33]), $J_1(\mathbf{f})$ is the regularization function (derived from a Gibbs prior) and β is a positive regularization parameter. Some regularization functions depend on another parameter (that we call δ). In Appendix A we describe the regularization functions $J_1(\mathbf{f})$ available in `AIRY`. The complete description of the regularizations as well as some discussions on the choice of the regularization parameters can be found, e.g., in Prato et al[27]. The maximum a posteriori (MAP) estimates of the unknown object $\mathbf{f}$ are the solutions of the minimization problem $\mathbf{f}_\beta = \arg\min_{\mathbf{f}\in\Omega} J_\beta(\mathbf{f}; \mathbf{g})$, where Ω is either the nonnegative orthant or the set of solutions satisfying the flux constraint, where the flux is defined as:

$$c = \frac{1}{p} \sum_{j=1}^{p} \sum_{\mathbf{m}\in S} [\mathbf{g}_j(\mathbf{m}) - \mathbf{b}_j(\mathbf{m})]. \tag{3}$$

The solution can be obtained by the Split Gradient Method[34] (SGM) or via SGP. In all cases the algorithm is iterative and it must be stopped following a given criterion. For all the methods based on Poisson data, i.e. RL, OSEM, and SGP, the stopping rules are*:

#1 Set a maximum number of iterations and stop the selected algorithm when $k \geq k_{\max}$.

#2 Stop the iterations when the relative difference in ℓ_2-norm of two consecutive iterates is smaller than a given tolerance (ν): $||\mathbf{f}^{(k)} - \mathbf{f}^{(k-1)}|| \leq \nu ||\mathbf{f}^{(k)}||$.

#3 Stop the iterations when the objective function J_β (or J_0 in the case of no-regularization) is approximately constant, given a tolerance ν (usually $\nu \ll 1$, for example 10^{-6}): $\left|J_\beta(\mathbf{f}^{(k)}; \mathbf{g}) - J_\beta(\mathbf{f}^{(k-1)}; \mathbf{g})\right| \leq \nu J_\beta(\mathbf{f}^{(k)}; \mathbf{g})$.

#4 Stop the iterations when the *discrepancy* function, defined as $D^{(k)} = 2 \cdot J_0(\mathbf{f}^{(k)}; \mathbf{g})/(pN)$ crosses a given value (that should be 1, in the case of pure Poisson data[35]), where N is the total number of pixels in S.

#5 Stop when the restoration error, defined as $\rho^{(k)} = ||\mathbf{f}^{(k)} - \tilde{\mathbf{f}}|| \;/\; ||\tilde{\mathbf{f}}||$ reaches a minimum value. This stopping rule can be applied only in the case of simulation, when the so-called *ground truth* $\tilde{\mathbf{f}}$ is known.

In Fig. 2 we show the block diagram of the `DEC` module. The main box is for the deconvolution and it is indicated by SGP, but of course any other method can be selected here. The algorithm is initialized by

*Both first rule and last one are also available in the case of ISRA and OS-ISRA

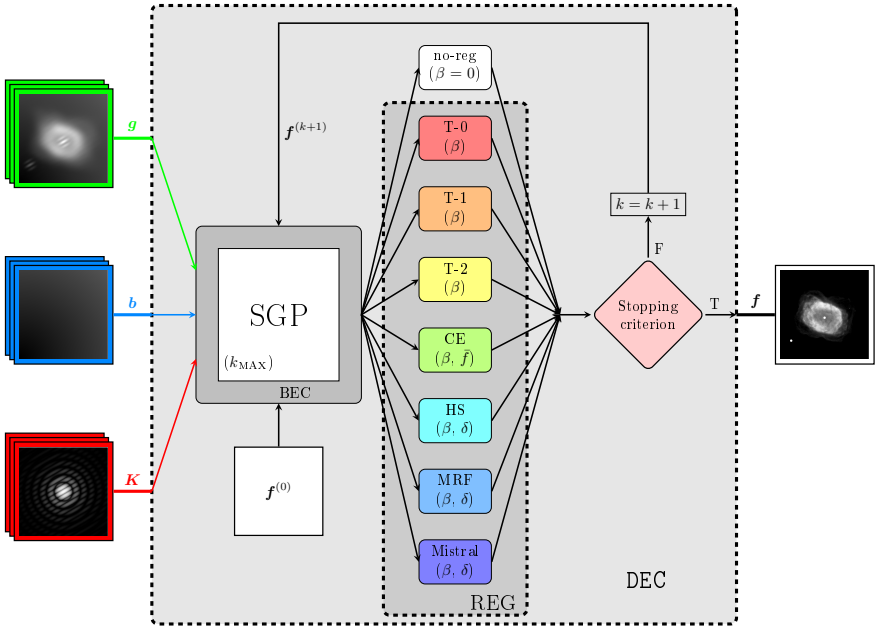

Figure 2. The block diagram of the `DEC` module. The inputs of the method are: the image(s) **g**, the PSF(s) **K**, and the background **b**. Even if the background is set within the `PRE` module, here is shown as one of the inputs of the method as actually it is. Each internal block is dedicated to a particular task: the main code (indicated by SGP), the boundary effect correction (BEC), one of proposed regularizations (and the case of no-regularization) described in Tab. A, and the stopping rules. The output of the module is the reconstructed oject **f**.

default by a constant array satisfying the flux constant c, but the user can provide a different initialization. The boundary effect correction is indicated with BEC and surrounds the main box. Starting from this, one of the eight regularizations (considering also the particular case of no-regularization) can be chosen. Each block shows the parameters (if any) that the user must provide as an input. Finally one stopping rule must be satisfied in order to stop the iterations and obtain the reconstructed object.

3. THE MULTI-COMPONENT DECONVOLUTION MODULE

3.1 Description of the method

In this section we briefly describe the methods for deconvolving high dynamic range images. We already developed[8,36] an algorithm, called multi-component Richardson-Lucy (MCRL) and in the paper[27] an application of SGP to this situation is shown. Since it is the first time that we describe this method within the package `AIRY`, we give here a summary of the main ideas.

Firstly, we assume that the unknown object **f** is the sum of two *components*: the point-like part $\mathbf{f}_P$ containing the bright sources of the object superimposed on the extended and smooth part $\mathbf{f}_E$. Moreover we assume to know the positions of the bright sources, i.e. we can provide a mask $\mathbf{M}_P$ which is 1 in the pixels of the sources and 0 elsewhere. Alternatively, we can set the mask to 1 in small regions around the known positions.

In Fig. 3 we show the block diagram of the multi-component method (MCM) that uses a core code based on either MCRL or the modification of SGP developed for taking into account this model. By analogy with MCRL, we call this new algorithm MCSGP. The user must provide, besides the standard inputs (i.e. the image(s), the PSF(s), and the backgroud(s)), also the mask $\mathbf{M}_P$. The algorithm computes the N_P positions of the bright sources (indexed by $\mathbf{i}_P$) and defines the default initial arrays: an $N \times N$ image $\mathbf{f}_E^{(0)}$ and an N_P vector $\mathbf{f}_P'^{(0)}$. As usually, the algorithm can also be initialized with user-defined arrays. The main box contains the core algorithm (as we said, both MCSGP and MCRL are given), that can be extended by the boundary effect correction (BEC)

method, as shown by the surrounding box. Regularizations can be applied to the diffuse component, as in the previous case, while no-regularization is needed for the pointwise part. Again, the iterations run until a stopping rule is satisfied and the algorithm gives the two reconstructed components, i.e. $\mathbf{f}_E$ and $\mathbf{f}_P$, as $N \times N$ arrays. One can compute the final reconstruction as the sum of the two components. The method is contained within the brand-new module called `MCD` that will be described in the next section.

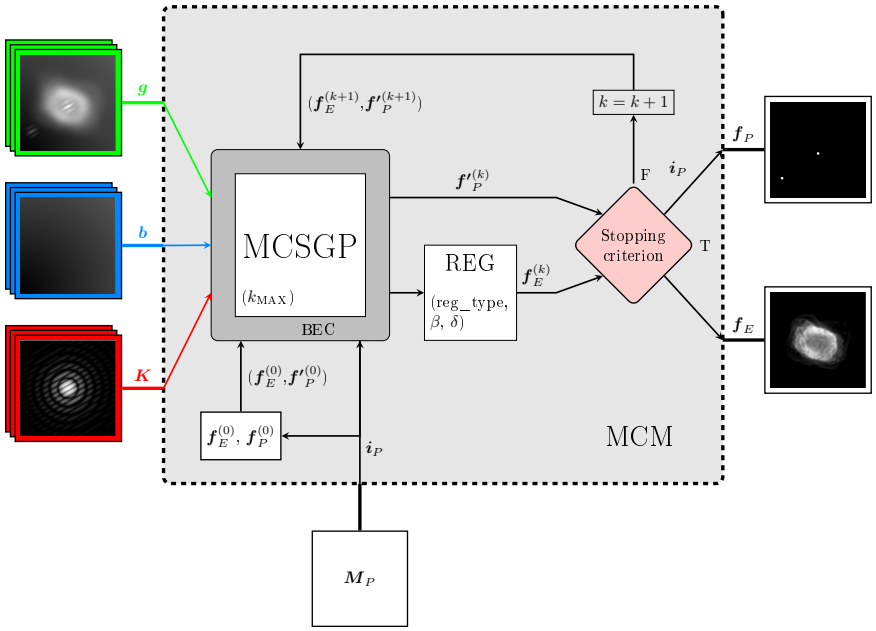

Figure 3. The block diagram of the Multi-Component Method (MCM). The inputs of the method are described in Fig. 2. The user must also provide the mask $\mathbf{M}_P$ (see text) that is used for the definition of the index $\mathbf{i}_P$ of the positions of the bright sources. Each internal block is dedicated to a particular task: the main code (indicated by MCSGP, but also MCRL is available), the boundary effect correction (BEC), one of proposed regularizations (and the case of no-regularization), and the stopping rules. The output of the module is the pair of the two components.

3.2 The module MCD

The `MCD - Multi-Component Deconvolution` module is a new module of the package `AIRY` and it is designed as a clone of `DEC`, since they are very similar for aiming and settings. Nonetheless, we need two separate modules because the outputs of the two algorithms are different: `DEC` gives one reconstructed object (one output in the worksheet of the `CAOS PSE` to be linked to other modules), while `MCD` provides the two components. Since also the core code is different, we need to add a new module to the list. As usual, the input image(s) and the PSF(s) can be set in the input part of the module, while the background definition comes from the module `PRE`. One additional input, that is mandatory within `MCD`, is the mask $\mathbf{M}_P$, stored in a FITS file that can be loaded within the GUI of the module. As mentioned before, the user can also provide different initialization arrays. As concerns the stopping rules, all the five criteria are available within the `MCD` module, with the only exception that the restoration error is computed on the diffuse part and not on the entire object. Therefore, in that case, the stopping rule is:

#5 Stop when the restoration error, defined as $\rho^{(k)} = ||\mathbf{f}_E^{(k)} - \tilde{\mathbf{f}_E}|| \ / \ ||\tilde{\mathbf{f}_E}||$ reaches a minimum value. This stopping rule can be applied only in the case of simulation, when the so-called *ground truth* $\tilde{\mathbf{f}_E}$ is known.

Finally, the discrepancy and the objective function values at each iteration can be saved as ASCII files. In the case of simulation, the restoration error (computed on the diffuse component) at each iteration can be saved.

4. THE MULTI-STEP ALGORITHM

4.1 Description of the algorithm

In some cases the MCM is not directly applicable. For example, the positions of the bright spots are not known or they can not directly found on the observed images. In particular, this is true in the case of Io images acquired with the LBT/LBTI LMIRcam instrument that our group already reconstructed[37,38]. For this reason, we developed a multi-step method (MSM) that is described for the first time in the mentioned paper[27] and that we report here for sake of completeness.

- Step 1 - The input image is deconvolved by using a standard algorithm, for example SGP with no-regularization (or with an edge-preserving regularization and a small parameter β). The algorithm can be pushed to convergence, i.e. until the stopping rule #3 is satisfied. The result is a de-blurred version of the image and can be used for retrieving the centroids of the bright spots.
- Step 2 - The centroids of the bright spots are used for defining the mentioned mask $\mathbf{M}_P$. In some cases small regions around the centroids can be considered instead of the single pixel. In those pixels the mask must be set to 1 and 0 elsewhere.
- Step 3 - This is the crucial step in which MCM is applied by using the previous mask. A suitable regularizer with a good choice of the regularization parameter(s) must be set in order to appropriately reconstruct the diffuse part of the object. The reconstruction of the point-like component is not very important in this step and we do not consider it in the following.
- Step 4 - The result of the previous step (i.e. $\mathbf{f}_E$) is used to re-define the background input of a standard deconvolution algorithm. Indeed, the algorithm computes

$$\mathbf{b}'_j = \mathbf{b}_j + \mathbf{K}_j * \mathbf{f}_E \ .$$

  The unknown object to be reconstructed becomes $\mathbf{h} = \mathbf{f} - \mathbf{f}_E$ and consists of the bright sources, since the algorithm concentrates the flux in a few regions. Again, the algorithm must be pushed to convergence. The block diagram of this last step is shown in Fig. 4. At the end of this step the complete object $\mathbf{f}$ can be obtained by adding the diffuse component to the result.

Since the last step uses a standard algorithm, we remark that some modifications have been introduced within the `DEC` module and in particular the possibility of loading the FITS file containing the diffuse component as an optional input.

4.2 Example projects

The steps described above are naturally implemented within `AIRY` in some example projects provided together with the package. The examples are called `MultiStepMethod_Example_Step`i where $i = 1, 3, 4$ is the number of the step. We remark that, for Step 2, no deconvolution (and no computation) is necessary, since the user has only to create the mask $\mathbf{M}_P$ and to save it into a FITS file.

For these example projects we use a simulation of a Io-like object at M-band (4.8 μm) that is obtained considering nine hot spots superimposed to a variable smooth surface. The object is convolved to the input PSF modelling the Keck-II PSF in M-band. The result is perturbed with Poisson noise. The object, the PSF and the blurred and noisy image are shown in Fig. 5.

In the first example project (i.e. the first step of our MSM algorithm) we apply a non-regularized SGP, stopped with a tolerance $\nu = 10^{-6}$. The result shows a number of artifacts around the bright spots (see the first panel of Fig. 6) so that the further steps are necessary in order to reconstruct the object. From the result of this first step, we can obtain the position of the nine hot-spots and we can define $\mathbf{M}_P$ (step 2, second panel of Fig. 6).

The next example project (that manages the third step of the method) contains the new module `MCD`, used for the multi-component reconstruction of the two parts of the object. The user can try different regularized

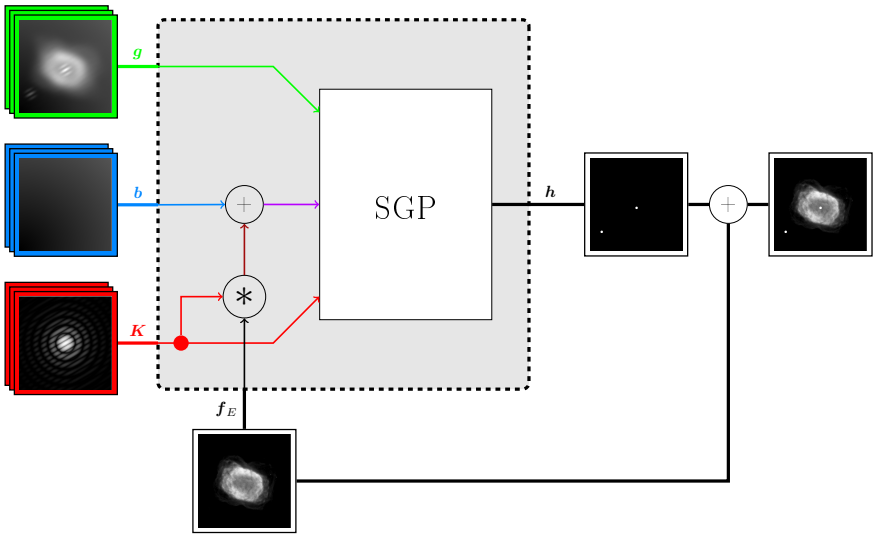

Figure 4. The block diagram of the last step of the Multi-Step Method (MSM). The inputs of the method are described in Fig. 2, with the addition of the extended component $\mathbf{f}_E$ obtained from the third step (see text). Within the algorithm this component is convolved with the PSF(s) **K** and added to the background **b**. This latter result is used as the new background in a standard deconvolution (SGP is shown in the box, but any other methods can be used). The restored object **h** is the output of the method and the complete object can be obtained by adding the diffuse component.

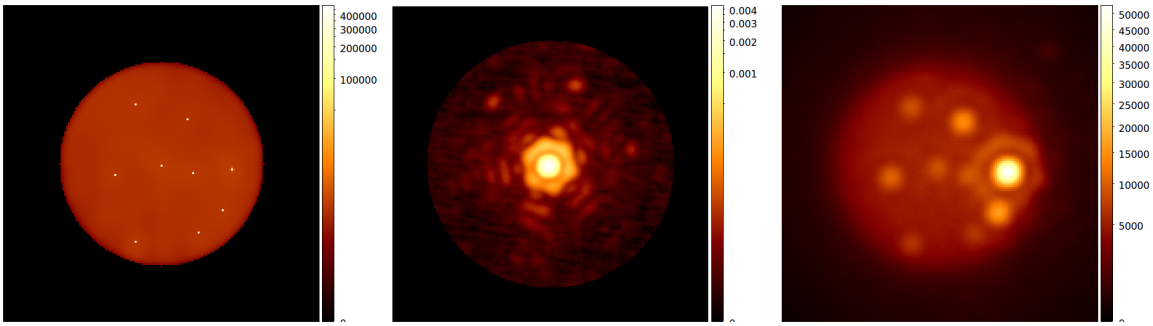

Figure 5. Simulated Io-like image. *(Left)* The model of the surface with the addition of the nine bright spots. *(Middle)* The model of the PSF. *(Right)* The blurred and noisy image.

algorithms keeping in mind that the best results are obtained with edge-preserving functions (i.e. MRF, Mistral, or HS functions) and that the choice of the parameters must be finely tuned. With our suggestions (MRF and $\beta = 10^{-2}, \delta = 10$) the diffuse part of Io is reconstructed with a small reconstruction error (around 7%). The result is shown in the third panel of Fig. 6.

In the last example project (corresponding to the fourth step of MSM) the result of the previous step is loaded within `DEC` as an optional input and the algorithm (we suggest again to use no-regularized SGP) can be stopped with $\nu = 10^{-7}$. In this last step, the best results are obtained if the flux constraint is activated on the GUI. In the last panel of Fig. 6 we show the result of the fourth step to which we added the smooth surface of the previous step.

5. CONCLUSIONS AND FUTURE DEVELOPMENTS

In this paper we presented the new version of the `Software Package AIRY`, an IDL-based tool for the simulation and the restoration of post AO images. `AIRY` is a package of the `CAOS PSE`, that recently has been renewed and simplified.

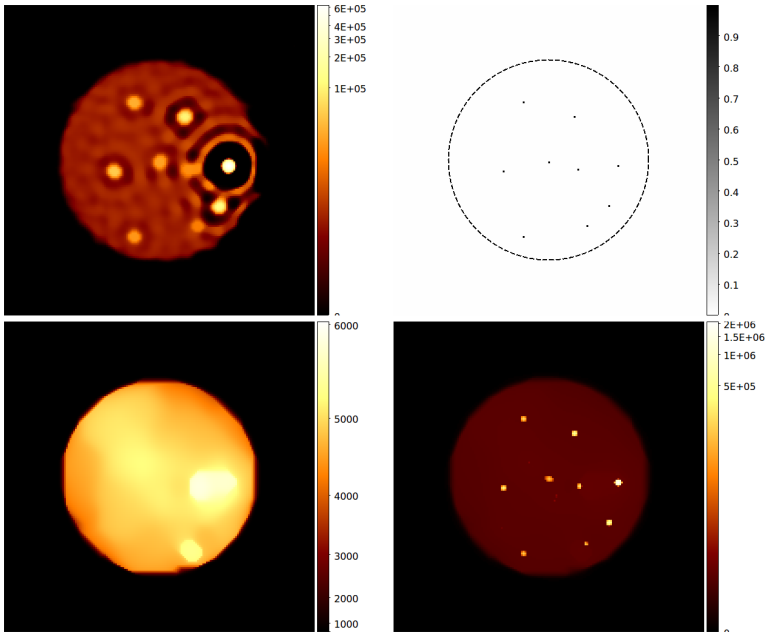

Figure 6. Reconstructions of the Io-like image during the four steps. *(Upper left)* The result of the first step has several artifacts around the bright spots. *(Upper right)* The mask $\mathbf{M}_P$ in reverse B/W scale. The dashed circle shows the limb of Io: it is shown for sake of clarity and must not be included in the mask. *(Lower left)* The reconstruction of the surface as obtained at the third step with MRF regularization and $\beta = 10^{-2}, \delta = 10$. *(Lower right)* The complete reconstruction (surface plus the result of the last step).

Thanks to the application of the SGP method to the case of different regularization functions, the renewed `DEC` module contains efficient methods for the deconvolution. Moreover, a new module called `MCD` has been developed for the restoration of high dynamic range images. Based on our multi-component algorithm, both MCSGP and MCRL are available for reconstructing the point-like and the diffuse part of the unknown object. Finally we described the multi-step method, particularly useful in the case of Io like images. Some example projects are provided together with the package.

Future perspectives of this work include the use of efficient libraries for FFT computation (based on the well known FFTW library) and the develop of a de-noising module, following the approach presented in Bertero et al[26].

The `Software Package AIRY` together with the `CAOS PSE` can be freely downloaded from:

http://lagrange.oca.eu/caos/

APPENDIX A. REGULARIZATION FUNCTIONS AVAILABLE IN AIRY

We describe here the seven regularization functions $J_1(\mathbf{f})$ available in `AIRY`. In Tab. 3, the term $\mathbf{D}^2(\mathbf{n})$ is the square of the discrete gradient (first row), while Δ (second row) denotes the discrete Laplacian, $\bar{\mathbf{f}}$ (second row) is a reference image, and $|\mathbf{D}(\mathbf{n})|$ (third row) is the magnitude of the discrete gradient. Finally, $\mathcal{N}(\mathbf{n})$ (last row) is a symmetric neighborhood made up of the eight first neighbors of $\mathbf{n}$ and $\epsilon(\mathbf{n}')$ is equal to 1 for the horizontal and vertical neighbors and equal to $\sqrt{2}$ for the diagonal ones. For more details, see Prato et al[27].

ACKNOWLEDGMENTS

This work has been partially supported by MIUR (Italian Ministry for University and Research), under the projects FIRB - Futuro in Ricerca 2012 (contract RBFR12M3AC) and PRIN 2012 (contract 2012MTE38N). The Italian GNCS — INdAM (Gruppo Nazionale per il Calcolo Scientifico — Istituto Nazionale di Alta Matematica) is also acknowledged.

Table 3. Regularization functions available in `AIRY`.

Zeroth order Tikhonov (T-0): $$J_1(\mathbf{f}) = \frac{1}{2}\sum_{\mathbf{n}} \lvert\mathbf{f}(\mathbf{n})\rvert^2$$	First order Tikhonov (T-1): $$J_1(\mathbf{f}) = \frac{1}{2}\sum_{\mathbf{n}} \mathbf{D}^2(\mathbf{n})$$
Second order Tikhonov (T-2): $$J_1(\mathbf{f}) = \frac{1}{2}\sum_{\mathbf{n}} (\Delta\mathbf{f})(\mathbf{n})^2$$	Cross-Entropy (CE)[39,40]: $$J_1(\mathbf{f}) = J_0(\mathbf{f},\bar{\mathbf{f}}) = \sum_{\mathbf{n}} \left\{\mathbf{f}(\mathbf{n}) \ln\left(\frac{\mathbf{f}(\mathbf{n})}{\bar{\mathbf{f}}(\mathbf{n})}\right) + \bar{\mathbf{f}}(\mathbf{n}) - \mathbf{f}(\mathbf{n})\right\}$$
Hypersurface (HS)[41]: $$J_1(\mathbf{f}) = \sum_{\mathbf{n}} \sqrt{\delta^2 + \mathbf{D}^2(\mathbf{n})} \quad , \quad \delta > 0$$	MISTRAL regularization[42]: $$J_1(\mathbf{f}) = \sum_{\mathbf{n}} \lvert\mathbf{D}(\mathbf{n})\rvert - \delta \ln\left(1 + \frac{\lvert\mathbf{D}(\mathbf{n})\rvert}{\delta}\right) \quad , \quad \delta > 0$$
Markov random field (MRF)[43]: $$J_1(\mathbf{f}) = \frac{1}{2}\sum_{\mathbf{n}} \sum_{\mathbf{n}'\in\mathcal{N}(\mathbf{n})} \sqrt{\delta^2 + \left(\frac{\mathbf{f}(\mathbf{n}) - \mathbf{f}(\mathbf{n}')}{\epsilon(\mathbf{n}')}\right)^2} \quad , \quad \delta > 0$$	

REFERENCES

[1] Correia, S., Carbillet, M., Boccacci, P., Bertero, M., and Fini, L., "Restoration of interferometric images: I. the software package AIRY," *Astron. Astrophys.* **387**, 733–743 (2002).

[2] Richardson, W. H., "Bayesian based iterative method of image restoration," *J. Opt. Soc. Am.* **62**(1), 55–59 (1972).

[3] Lucy, L. B., "An iterative technique for the rectification of observed distributions," *Astron. J.* **79**, 745–754 (1974).

[4] Daube-Witherspoon, M. E. and Muehllehner, G., "An Iterative Image Space Reconstruction Algorthm Suitable for Volume ECT.," *IEEE transactions on medical imaging* **5**(2), 61–6 (1986).

[5] Carbillet, M., Vérinaud, C., Guarracino, M., Fini, L., Lardière, O., Roux, B. L., Puglisi, A. T., Femenía, B., Anconelli, A. R. B., Bertero, M., and Boccacci, P., "Caos – a numerical simulation tool for astronomical adaptive optics (and beyond)," in [*Advancements in Adaptive Optics*], Bonaccini, D., Ellerbroek, B., and Ragazzoni, R., eds., *Proc. SPIE* **5490 (2)**, 550 (2004).

[6] Carbillet, M., Desiderà, G., Augier, E., La Camera, A., Riccardi, A., Boccaletti, A., Jolissaint, L., and Kadir, D. A., "The caos problem-solving environment: recent developments," in [*Adaptive Optics Systems II*], Ellerbroek, B., Hart, M., Hubin, N., and Wizinowich, P. L., eds., *Proc. SPIE* **7736**, 773644 (2010).

[7] Carbillet, M., La Camera, A., and et al., "The software package caos 7.0: enhanced modelling of astronomical adaptive optics systems," in [*Adaptive Optics Systems V*], Marchetti, E., Close, L. M., and Véran, J.-P., eds., *Proc. SPIE* **9909**, 9909–319 (2016).

[8] La Camera, A., Antoniucci, S., Bertero, M., Boccacci, P., Lorenzetti, D., Nisini, B., and Arcidiacono, C., "Reconstruction of high dynamic range images: Simulations of lbt observations of a stellar jet, a pathfinder study for future ao-assisted giant telescopes," *Publications of the Astronomical Society of the Pacific* **126**(936), pp. 180–193 (2014).

[9] Fini, L., Carbillet, M., and Riccardi, A., "The CAOS Application Builder," *Astronomical Data Analysis Software and Systems X* **238**, 253 (2001).

[10] Desiderà, G. and Carbillet, M., "Strehl-constrained iterative blind deconvolution for post-adaptive-optics data," *Astron. Astrophys.* **507**(3), 1759–1762 (2009).

[11] Prato, M., La Camera, A., Bonettini, S., and Bertero, M., "A convergent blind deconvolution method for post-adaptive-optics astronomical imaging," *Inverse Probl.* **29**(6), 065017 (2013).

[12] Prato, M., La Camera, A., Bonettini, S., Rebegoldi, S., Bertero, M., and Boccacci, P., "A blind deconvolution method for ground based telescopes and fizeau interferometers," *New Astron.* **40**, 1–13 (Oct. 2015).

[13] Carbillet, M., La Camera, A., Deguignet, J., Prato, M., Bertero, M., Aristidi, E., and Boccacci, P., "Strehl-constrained reconstruction of post-adaptive optics data and the Software Package AIRY, v. 6.1," in [*Adaptive Optics Systems IV*], Marchetti, E., Close, L. M., and Véran, J.-P., eds., *Proc. SPIE* **9148**, 91484U (2014).

[14] Antoniucci, S., La Camera, A., Nisini, B., Giannini, T., Lorenzetti, D., Paris, D., and Sani, E., "The HH34 outflow as seen in [Fe II] 1.64 μm by LBT-LUCI," *Astronomy & Astrophysics* **566**, A129 (jun 2014).

[15] Bertero, M. and Boccacci, P., "Application of the OS-EM method to the restoration of LBT images," *Astron. Astrophys. Suppl. Series* **144**(1), 181–186 (2000).
[16] Anconelli, B., Bertero, M., Boccacci, P., Carbillet, M., and Lanteri, H., "Restoration of interferometric images - iii. efficient richardson-lucy methods for linc-nirvana data reduction," *Astron. Astrophys.* **430**, 731–738 (2005).
[17] La Camera, A., Carbillet, M., Olivieri, C., Boccacci, P., and Bertero, M., "AIRY: a complete tool for the simulation and the reconstruction of astronomical images," in [*Optical and Infrared Interferometry III. Proceedings of the SPIE*], 84453E, Univ. degli Studi di Genova (Italy) (2012).
[18] Shepp, L. A. and Vardi, Y., "Maximum likelihood reconstruction for emission tomography," *IEEE Trans. Med. Imaging* **MI-1**, 587–687 (1982).
[19] Bonettini, S., Zanella, R., and Zanni, L., "A scaled gradient projection method for constrained image deblurring," *Inverse Probl.* **25**(1), 015002 (2009).
[20] Biggs, D. S. C. and Andrews, M., "Iterative blind deconvolution of extended objects," in [*International Conference on Image Processing*], 454–457, IEEE Comput. Soc (1997).
[21] Biggs, D. S. C. and Andrews, M., "Asymmetric iterative blind deconvolution of multi-frame images," in [*Advanced Signal Processing Algorithms, Architectures, and Implementations VIII*], Franklin, T. L., ed., *Proc. SPIE* **3461**, 328–338 (1998).
[22] Anconelli, B., Bertero, M., Boccacci, P., and Carbillet, M., "Restoration of interferometric images. IV. An algorithm for super-resolution of stellar systems," *Astron. Astroph.* **431**, 747–755 (2005).
[23] Carbillet, M., La Camera, A., Chesneau, O., Millour, F., Girard, J., and Prato, M., "Deconvolution-based super resolution for post-AO data," in [*Proceedings of the Third AO4ELT Conference. Firenze*], 104 (2013).
[24] Bertero, M. and Boccacci, P., "A simple method for the reduction of boundary effects in the Richardson-Lucy approach to image deconvolution," *Astron. Astrophys.* **437**, 369–374 (2005).
[25] Anconelli, B., Bertero, M., Boccacci, P., Carbillet, M., and Lantéri, H., "Reduction of boundary effects in multiple image deconvolution with an application to LBT LINC-NIRVANA," *Astron. Astrophys.* **448**, 1217–1224 (2006).
[26] Bertero, M., Boccacci, P., La Camera, A., Olivieri, C., and Carbillet, M., "Imaging with LINC-NIRVANA, the Fizeau interferometer of the Large Binocular Telescope: state of the art and open problems," *Inverse Probl.* **27**(11), 113011 (2011).
[27] Prato, M., La Camera, A., Boccacci, P., and Bertero, M., "Reconstruction of high-dynamic range Poisson data with an application to Io imaging," *Inverse Prob.* **submitted** (2016).
[28] Bonettini, S. and Prato, M., "Nonnegative image reconstruction from sparse Fourier data: a new deconvolution algorithm," *Inverse Probl.* **26**(9), 095001 (2010).
[29] Bonettini, S. and Prato, M., "New convergence results for the scaled gradient projection method," *Inverse Probl.* **31**, 095008 (Sept. 2015).
[30] Porta, F., Prato, M., and Zanni, L., "A new steplength selection for scaled gradient methods with application to image deblurring," *J. Sci. Comput.* **65**, 895–919 (Dec. 2015).
[31] Prato, M., Cavicchioli, R., Zanni, L., Boccacci, P., and Bertero, M., "Efficient deconvolution methods for astronomical imaging: algorithms and IDL-GPU codes," *Astron. Astrophys.* **539**, A133 (2012).
[32] Snyder, D. L., Helstrom, C. W., Lanterman, A. D., Faisal, M., and White, R. L., "Compensation for readout noise in CCD images," *J. Opt. Soc. Am. A* **12**(2), 272–283 (1995).
[33] Csiszár, I., "Why least squares and maximum entropy? An axiomatic approach to inference for linear inverse problems," *Ann. Stat.* **19**(4), 2032–2066 (1991).
[34] Lantéri, H., Roche, M., and Aime, C., "Penalized maximum likelihood image restoration with positivity constraints: multiplicative algorithms," *Inverse Probl.* **18**(5), 1397–1419 (2002).
[35] Bertero, M., Boccacci, P., Talenti, G., Zanella, R., and Zanni, L., "A discrepancy principle for Poisson data," *Inverse Probl.* **26**(10), 10500 (2010).
[36] La Camera, A., Antonucci, S., Bertero, M., Boccacci, P., Lorenzetti, D., and Nisini, B., "Image reconstruction for observations with a high dynamic range: LINC-NIRVANA simulations of a stellar jet," in [*Optical and Infrared Interferometry III*], Delplancke, F., Rajagopal, F. J. K., and Malbet, F., eds., *Proc. SPIE* **8455**, 84553D (2012).
[37] Leisenring, J. M., Hinz, P. M., Skrutskie, M. F., Skemer, A., Woodward, C. E., Veillet, C., Arcidiacono, C., Bailey, V., Bertero, M., Boccacci, P., Conrad, A., de Kleer, K., de Pater, I., Defrère, D., Hill, J., Hofmann, K.-H., Kaltenegger, L., La Camera, A., Nelson, M. J., Schertl, D., Spencer, J., Weigelt, G., and Wilson, J. C., "Fizeau interferometric imaging of Io volcanism with LBTI/LMIRcam," in [*Optical and Infrared Interferometry IV*], *Proc. SPIE* **9146**, 91462S (2014).
[38] Conrad, A., de Kleer, K., Leisenring, J., La Camera, A., Arcidiacono, C., Bertero, M., Boccacci, P., Defrère, D., de Pater, I., Hinz, P., Hofmann, K.-H., Kürster, M., Rathbun, J., Schertl, D., Skemer, A., Skrutskie, M., Spencer, J., Veillet, C., Weigelt, G., and Woodward, C. E., "Spatially Resolved M-Band Emission from Io's Loki Patera-Fizeau Imaging at the 22.8m LBT," *Astron. J.* **149**, 1–9 (Apr. 2015).
[39] Byrne, C. L., "Iterative image reconstruction algorithms based on cross-entropy minimizatio," *IEEE Trans. Image Proc.* **IP-2**, 96–103 (1993).

[40] Carasso, A. S., "Linear and nonlinear image deblurring: a documented study," *SIAM J. Numer. Anal.* **36**(6), 1659–1689 (1999).
[41] Charbonnier, P., Blanc-Féraud, L., Aubert, G., and Barlaud, M., "Deterministic edge-preserving regularization in computed imaging," *IEEE T. Image Process.* **6**, 298–311 (1997).
[42] Mugnier, L. M., Fusco, T., and Conan, J.-M., "Mistral: a myopic edge-preserving image restoration method, with application to astronomical adaptive-optics-corrected long-exposure images," *J. Opt. Soc. Am.* **A-21**(4), 1841–1854 (2004).
[43] Geman, S. and Geman, D., "Stochastic relaxation, Gibbs distributions and the Bayesian restoration of images," *IEEE Trans. Pattern Anal. Mach. Intell.* **6**, 721–741 (Nov. 1984).